

Endoplasmic Reticulum Stress-Activated Transcription Factor ATF6 α Requires the Disulfide Isomerase PDIA5 To Modulate Chemoresistance

Arisa Higa,^{a,*} Said Taouji,^a Stéphanie Lhomond,^a Devon Jensen,^b Martin E. Fernandez-Zapico,^c Jeremy C. Simpson,^d Jean-Max Pasquet,^e Randy Schekman,^b Eric Chevet^a

INSERM U1053, Université Bordeaux Segalen, Bordeaux, France^a; Department of Molecular and Cell Biology, University of California at Berkeley, Berkeley, California, USA^b; Schulze Center for Novel Therapeutics, Division of Oncology Research, Mayo Clinic, Rochester, Minnesota, USA^c; School of Biology & Environmental Science and Conway Institute of Biomolecular & Biomedical Research, University College Dublin, Belfield, Dublin, Ireland^d; INSERM U1035, Université Bordeaux Segalen, Bordeaux, France^e

ATF6 α , a membrane-anchored transcription factor from the endoplasmic reticulum (ER) that modulates the cellular response to stress as an effector of the unfolded-protein response (UPR), is a key player in the development of tumors of different origin. ATF6 α activation has been linked to oncogenic transformation and tumor maintenance; however, the mechanism(s) underlying this phenomenon remains elusive. Here, using a phenotypic small interfering RNA (siRNA) screening, we identified a novel role for ATF6 α in chemoresistance and defined the protein disulfide isomerase A5 (PDIA5) as necessary for ATF6 α activation upon ER stress. PDIA5 contributed to disulfide bond rearrangement in ATF6 α under stress conditions, thereby leading to ATF6 α export from the ER and activation of its target genes. Further analysis of the mechanism demonstrated that PDIA5 promotes ATF6 α packaging into coat protein complex II (COPII) vesicles and that the PDIA5/ATF6 α activation loop is essential to confer chemoresistance on cancer cells. Genetic and pharmacological inhibition of the PDIA5/ATF6 α axis restored sensitivity to the drug treatment. This work defines the mechanisms underlying the role of ATF6 α activation in carcinogenesis and chemoresistance; furthermore, it identifies PDIA5 as a key regulator ATF6 α -mediated cellular functions in cancer.

Protein folding in the endoplasmic reticulum (ER) can be particularly affected by the presence of mutations in secretory proteins or by dynamic changes in the cellular microenvironment, events which are often encountered in cancers. In the ER, these events are sensed by specific sensors, which in turn trigger select signaling pathways, collectively named the unfolded-protein response (UPR) (1). The UPR is an adaptive response that allows the cells to either overcome the stress or promote cell death in the case of overwhelming burden (1). Three ER-resident proteins, namely, the protein kinase PKR-like ER kinase (PERK), the inositol-requiring protein 1 α (IRE1 α), and the activating transcription factor 6 α (ATF6 α), have been identified as the major transducers of the UPR in mammals. They display an ER luminal domain that senses misfolded proteins and are activated by a common mechanism involving the dissociation of the ER chaperone BiP/GRP78. PERK is responsible for translational attenuation through the phosphorylation of the α subunit of the eukaryotic translation initiation factor 2 (eIF2 α) (2). IRE1 α mediates the unconventional splicing of X-box binding protein 1 (*Xbp1*) mRNA (3) as well as mRNA expression levels through regulated IRE1 α -dependent mRNA decay (RIDD) (4) and controls the activation of the c-jun N-terminal kinase (JNK) pathway. The third arm of the UPR is controlled by ATF6 α . This membrane-anchored transcription factor is a type II transmembrane protein regulated by intramembrane proteolysis by the Golgi apparatus-localized site 1 and site 2 proteases (S1P and S2P) upon ER stress (5). Indeed, upon ER stress, BiP dissociates from the luminal domain of ATF6 α , thereby unmasking both Golgi localization signals (6) and disulfide bonds between two conserved cysteine residues (7, 8). Although ATF6 α has been linked to cancer development (9, 10) or tumor dormancy (11), the precise underlying mechanisms remain unclear. To better characterize the ER molec-

ular mechanisms underlying ATF6 α activation processes in the ER and to evaluate their role(s) in cancer, we developed a functional ATF6 α activation screen using small interfering RNAs (siRNAs) targeting a panel of well-established cancer-relevant ER foldases (12, 13). We identify protein disulfide isomerase A5 (PDIA5) as an essential ER-localized regulator of ATF6 α activation allowing this transcription factor export from the ER upon stress. Moreover, using leukemia cells as a model, we show a novel role of this ATF6 α /PDIA5 axis in regulating resistance to imatinib. Collectively, our results identify a novel signaling pathway mediating chemoresistance in cancer cells, and this knowledge may help in the tailoring of future clinical studies.

MATERIALS AND METHODS

Cell culture and transfection. HeLa cells were cultured in Dulbecco's modified Eagle's medium (DMEM) supplemented with 10% fetal bovine serum (FBS) and penicillin-streptomycin (100 U/ml and 100 μ g/ml, respectively) at 37°C in a 5% CO₂ incubator. HeLa cells stably expressing 3 \times FLAG-ATF6 α (HeLa-ATF6 α) were generated and maintained as previously described (14). K562 and LAMA cells (imatinib resistant or imatinib

Received 6 November 2013 Returned for modification 30 November 2013

Accepted 10 February 2014

Published ahead of print 17 March 2014

Address correspondence to Eric Chevet, eric.chevet@inserm.fr.

* Present address: Arisa Higa, Medical Industry Translational Research Center, Fukushima Medical University, Fukushima, Japan.

Supplemental material for this article may be found at <http://dx.doi.org/10.1128/MCB.01484-13>.

Copyright © 2014, American Society for Microbiology. All Rights Reserved.

doi:10.1128/MCB.01484-13

sensitive) were maintained in RPMI 1640 medium containing 10% FBS and antibiotics. HeLa cells were transiently transfected with FLAG-ATF6 α or FLAG-ATF6 α -p50 using Lipofectamine and Plus reagents (Invitrogen) according to the manufacturer's protocols.

Antibodies and chemicals. Mouse monoclonal anti-FLAG M2 antibody was obtained from Sigma-Aldrich. Mouse monoclonal anti-ATF6 α antibody was from BioAcademia. Rabbit polyclonal anti-extracellular signal-regulated kinase 1 (anti-ERK1) antibody was from Santa Cruz Biotechnologies. Rabbit polyclonal anti-antigenin antibody was purchased from Abcam. Mouse monoclonal anti-PDIA5 and mouse monoclonal anti-KDEL were from Abnova and Stressgen, respectively. Rabbit anticalnexin (anti-CNX) antibodies were a kind gift from John Bergeron (McGill University, Montreal, Quebec, Canada). Polyclonal anti-enterobacterial repetitive intergenic consensus 53 (anti-ERGIC53), anti-ribophorin I, and anti-Sec22b antibodies were generated as described previously (14). Fluorescence-conjugated secondary antibodies were from Molecular Probes (Life Technologies). Imatinib mesylate (Gleevec; Novartis, Basel, Switzerland) was dissolved in dimethyl sulfoxide (DMSO) at a stock concentration of 250 mM, stored at -20°C , and subsequently diluted with serum-free culture medium prior to use. The PDI inhibitor 16F16 was purchased from Sigma (St. Louis, MO).

RNA interference. siRNAs were obtained from RNAi Co. and Ambion. The sequences of the siRNAs used in this study are described in Table S1 in the supplemental material. siRNA was delivered into HeLa, HeLa-ATF6 α , or K562 cells by reverse transfection using Lipofectamine RNAiMAX (Invitrogen) at an siRNA concentration of 12.5 or 25 nM.

In vitro budding assay. HeLa-ATF6 α cells were transfected with siRNAs against PDIA5 or a control. Seventy-two hours later, cells were permeabilized with 40 $\mu\text{g}/\text{ml}$ digitonin for 5 min on ice. Cells were then washed and incubated with an ATP-regenerating system (ATPr) (1 mM ATP, 40 mM creatine phosphate, 200 $\mu\text{g}/\text{ml}$ creatine phosphokinase, 50 μM GDP-mannose), 3 mM GTP, and 4 mg/ml rat liver cytosol in KHM buffer [110 mM potassium acetate (KOAc), 2 mM Mg(OAc) $_2$, and 20 mM HEPES, pH 7.2] for 1 h at 30°C . Rat liver cytosol was prepared as described previously (15). The vesicle fraction was separated from the donor microsome fraction by centrifugation at 12,000 rpm for 10 min. The supernatants were then centrifuged at 55,000 rpm for 25 min at 4°C to collect the vesicles. The pellets were solubilized with buffer C (10 mM Tris-HCl [pH 7.6], 100 mM NaCl, and 1% Triton X-100) and analyzed by immunoblotting using mouse monoclonal anti-ATF6 α (1:1,000), rabbit polyclonal anti-ERGIC53 (1:10,000), anti-ribophorin I (1:10,000), and anti-Sec22b (1:10,000).

Plasmids. Human ATF6 α cDNA was amplified by PCR from human liver total cDNA and cloned into p3 \times FLAG-CMV7.1 vector within the HindIII/SalI restriction sites. The FLAG-ATF6 α -p50 construct was derived from the above-mentioned plasmid. Human ATF6 α cDNA was digested with PvuII and subsequently ligated in the p3 \times FLAG vector. The resulting translation product corresponded to a FLAG-tagged ATF6 α -p50 protein. The dominant negative Sar1 [Sar1(DN)] plasmid was a kind gift from J. A. Lippincott-Schwartz (NIH, Bethesda, MD). To construct an siRNA-resistant PDIA5 cDNA (PDIA5r), the human PDIA5 cDNA was amplified by PCR and subcloned in pGEM-T Easy plasmid. Silent mutations were introduced by *in vitro* site-directed mutagenesis using the Stratagene QuikChange II XL site-directed mutagenesis kit in the regions that are targeted by siRNAs (PDIA5 sequence 5'-AGGATGATGCCGCAT replaced by 5'-AG~~A~~ATGATGCC~~A~~CAC~~C~~). The insert was then subcloned into pcDNA3 and sequence verified.

Indirect immunofluorescence. HeLa cells were plated on coverslips and transfected with FLAG-ATF6 α . Twenty-four hours posttransfection, cells were fixed in methanol at -20°C for 5 min and blocked with 3% bovine serum albumin (BSA) in immunofluorescence buffer [0.15 M NaCl, 2 mM EGTA, 1 mM MgCl $_2$, and 10 mM piperazine-*N,N'*-bis(2-ethanesulfonic acid) (PIPES)-Na, pH 7.2] for 30 min at room temperature. Cells were then incubated with primary (anti-FLAG, 1:500; anti-CNX, 1:500; or antigenin, 1:1,000) and secondary (Alexa Fluor 488-labeled

anti-mouse IgG or Alexa Fluor 568-labeled anti-rabbit IgG, 1:250) antibodies for 1 h. DNA was stained using Hoechst 33342 (Invitrogen) for 15 min. Coverslips were mounted on microscope slides using Fluoromount-G (Southern Biotech) and observed using a Leica TCS SP5 confocal microscope with a 63 \times oil immersion objective for fluorescence detection.

Immunoprecipitation and immunoblotting. To prepare whole-cell extracts, cells were washed twice with phosphate-buffered saline (PBS) and then incubated with radioimmunoprecipitation assay (RIPA) buffer (25 mM Tris-HCl [pH 7.5], 150 mM NaCl, 1% NP-40, 1% sodium deoxycholate, and 0.1% SDS) for 30 min on ice. Lysates were sonicated and centrifuged at 13,000 rpm for 20 min at 4°C . For immunoprecipitation, cells were rinsed twice and collected in ice-cold PBS. Cell pellets were then incubated with lysis buffer (50 mM Tris-HCl [pH 7.5] and 1% Triton X-100) for 30 min on ice and clarified by centrifugation at 13,000 rpm for 20 min at 4°C . For coimmunoprecipitation of ATF6 α with BiP, cells were transfected with Sar1(DN) after siRNA transfection and were lysed using lysis buffer. After preclearing using protein A- or protein G-Sepharose (GE Healthcare BioSciences), lysates were incubated overnight with anti-FLAG (1:200) antibodies at 4°C . The beads were then added to the immune complexes, precipitated for 1 h at 4°C with gentle rotation, and washed five times with lysis buffer. Immunoprecipitates were eluted with Laemmli sample buffer containing 50 mM dithiothreitol (DTT) for 10 min at 70°C . The proteins were analyzed by immunoblotting and detected using LumiGLO chemiluminescent substrate system (Kirkegaard & Perry Laboratories). Dilutions of primary antibodies used for immunoblotting were as follows: anti-ATF6 α , 1:1,000; anti-CNX, 1:2,000; anti-ERK, 1:1,000; anti-FLAG, 1:1,000; anti-KDEL, 1:1,000; and anti-PDIA5, 1:500.

qPCR. Total RNA was extracted from cells at 48 h after siRNA transfection using TRIzol reagent (Invitrogen) according to the manufacturer's instructions. cDNA was synthesized from the total RNA using the SuperScript first-strand synthesis system (Invitrogen) or a reverse transcription system (Promega) with oligo(dT) primer and amplified with Taq DNA polymerase (Invitrogen). For quantitative reverse transcription-PCR (qPCR), cDNA was analyzed with B-R SYBR green SuperMix (Quanta Bioscience) in a StepOnePlus system (Applied Biosystems). The primer sequences used for this experiment are shown in Table S2 in the supplemental material.

Mass spectrometry analyses and peptide quantification. HeLa-ATF6 α cells were transfected with siRNA against PDIA5 or a control in 150-mm-diameter dishes. Seventy-two hours posttransfection, cells were lysed in the presence of *N*-ethylmaleimide (NEM) using 25 mM Tris-HCl (pH 7.5), 150 mM NaCl, 1% NP-40, 1% sodium deoxycholate, and 0.3% SDS. Clarified lysates were then immunoprecipitated with anti-FLAG antibodies. Immunoprecipitates were eluted using a FLAG peptide, and the eluates were then resolved by nonreducing (NR) SDS-PAGE and the gel stained with Coomassie blue. The band corresponding to ATF6 α was excised and digested sequentially with trypsin and GluC. The extracted peptides were then analyzed and quantified by LTQ-Orbitrap (Thermo-Fisher) mass spectrometry as previously described using a label-free approach (16). Normalization was achieved by using three ATF6 α peptides systematically found in the experiments.

Cytotoxicity and apoptosis assays. Flow cytometry-based analysis of cell apoptosis was performed following staining of the cells with annexin V-fluorescein isothiocyanate (FITC) and propidium iodide (PI) using the annexin V-FITC kit (Beckman Coulter). The extent of apoptosis was quantified as the percentage of annexin V-positive cells. The extent of imatinib-induced apoptosis was assessed using the following formula: percent specific apoptosis = (test value $-$ control value) \times 100/(100 $-$ control value). Cell death was assessed using annexin V-fluorescein isothiocyanate-propidium iodide (annexin V FITC apoptosis kit; Beckman Coulter) according to the manufacturer's protocol. Sulforhodamine B (SRB) assays were performed as previously described (17).

Statistical analyses. Data are presented as means \pm standard errors of the means (SEM) from three separate experiments and were compared

using one-way analysis of variance (ANOVA) followed by Dunnett multiple-comparison tests. The level of significance was set at a *P* value of <0.05. All statistical analyses were performed using GraphPad Prism (version 5) statistical software (GraphPad Software, San Diego, CA).

RESULTS

ER-resident proteins regulate the activation of ATF6 α in response to ER stress. To study the mechanism regulating ATF6 α export from the ER to the Golgi apparatus and subsequent transport to the nucleus upon ER stress, we transiently expressed FLAG-tagged human ATF6 α (FLAG-ATF6 α) in HeLa cells and determined the localization of ATF6 α by immunofluorescence using anti-FLAG antibodies. To examine ATF6 α activation under ER stress, we used four known ER stress-inducing chemicals: dithiothreitol (DTT), a reducing agent; thapsigargin (Tg), a SERCA pump inhibitor; azetidine-2-carboxylic acid (Azc), a proline analog; and tunicamycin (Tun), an *N*-glycosylation inhibitor. As expected, ATF6 α was exported from the ER to the Golgi apparatus within 30 min and reached the nucleus after 2 h of DTT treatment. As shown in Fig. 1A, under basal conditions, ATF6 α colocalized with the ER marker calnexin (CNX), and following 1 h of DTT treatment, it colocalized with the Golgi complex marker giantin (Fig. 1A). Tg and Tun also induced the translocation of ATF6 α (see Fig. S1 in the supplemental material); however, the translocation kinetics were slower than with DTT treatment. Azc also promotes ATF6 α export but had the weakest effect on the trafficking of this transcription factor among the ER inducers used in the screening. Next, to confirm the activation of ATF6 α , we examined the cleavage of endogenous ATF6 α upon ER stress, an established marker for the activation of molecule. Consistent with the immunofluorescence data (Fig. 1A), immunoblot analysis showed that DTT was the strongest inducer of ATF6 α activation (Fig. 1B and C).

A reduction of intra- and intermolecular disulfide bonds in the ATF6 α luminal domain has been reported as an underlying molecular event leading to its ER export during ER stress (7). As a consequence, we designed a cell-based siRNA assay against ER-resident protein disulfide isomerases (PDIs) and thioredoxins and foldases to identify the enzyme(s) involved in disulfide bond formation and/or remodeling that is required for ATF6 α activation upon ER stress (see Fig. S2A in the supplemental material). Forty-eight hours after siRNA transfection, the cells were further transfected with FLAG-ATF6 α . Twenty-four hours later, the cells were treated with DTT to induced ER stress for 2 h. These cells were then immunostained using anti-FLAG and anti-CN or antigiantin antibodies. Cells expressing FLAG-ATF6 α protein (the number of cells counted ranged from 350 to 6,300) (Fig. 2A) were analyzed for the presence of tagged-ATF6 α in the ER, Golgi complex, and nucleus. The percentage of cells displaying both Golgi and nuclear localization of FLAG-ATF6 α in each siRNA-transfected cell population was determined and compared to that for the control siRNA-transfected cells (Fig. 2A). Both primary and validation screens revealed that only PDIA5 silencing led to altered export of ATF6 α to the Golgi complex upon DTT treatment (Fig. 2B). In order to confirm the effects of both PDIA5 siRNAs on their cognate target, we transfected each siRNA into HeLa cells and examined PDIA5 expression using immunoblotting (see Fig. S2B in the supplemental material). Transfection of each siRNA (siRNA-1 and siRNA-2) led to a significant decrease in PDIA5 expression compared to that with control siRNA. Both siRNAs

impacted neither CNX nor ERK1 expression, used as loading standards (see Fig. S2B in the supplemental material).

ER stress-induced ATF6 α activation was also monitored using immunoblotting in HeLa cells. This revealed that silencing of PDIA5 using the siRNAs used in the screen decreased ATF6 α cleavage upon DTT treatment (Fig. 2C; see Fig. S4A in the supplemental material [white arrowheads]), thus confirming the immunofluorescence data. Moreover, the effect of PDIA5 siRNA on ATF6 α cleavage was also observed in cells treated with the ER stress inducers Tg and Tun (see Fig. S3 and S4A in the supplemental material). Furthermore, silencing of PDIA3 or PDIA4 (see Fig. S4C in the supplemental material), two of the most abundant PDIs in the ER, did not affect ATF6 α activation upon DTT treatment (see Fig. S4B in the supplemental material), thus reinforcing the specificity of PDIA5 in this process.

PDIA5 silencing impairs ATF6 α transcriptional activity. To confirm the effect of PDIA5 silencing on ATF6 α activation and the subsequent impact on the transcriptional activation of ATF6 α target genes, we measured mRNA expression levels of ATF6 α target genes in control and PDIA5-silenced cells following DTT treatment (1 mM) using quantitative reverse transcription-PCR (qPCR). First we confirmed that the expression of *Pdia5* mRNA was attenuated by siRNA (Fig. 3A; see Fig. S5A in the supplemental material), and then we analyzed the expression of four ATF6 α bona fide target genes (*Ero1L β* , *Grp94*, *Orp150*, and *Herpud1*) (18, 19) and three UPR target genes (the spliced [*Xbp1s*] and unspliced [*Xbp1u*] forms of *Xbp1*, *Chop*, and *Gadd34*) upon DTT (Fig. 3A)- or Tg or Tun (see Fig. S5B in the supplemental material)-induced stress and/or silencing of PDIA5. This revealed that PDIA5 silencing prevented the induction of ATF6 α target genes upon ER stress without affecting the induction of the UPR targets, *Chop* and *Gadd34* (Fig. 3A and C; see Fig. S5B in the supplemental material). The total amount of *Xbp1s* mRNA decreased upon PDIA5 silencing (data not shown). However, this may account for the fact that ATF6 α also regulates the expression of *Xbp1* mRNA (3). This was confirmed by the fact that the induction of *Xbp1* mRNA splicing efficiency upon ER stress remained identical in control and PDIA5-silenced cells (Fig. 3B). These results established the requirement for an intact PDIA5 for the ATF6 α activation upon ER stress. To further ensure that the observed effect was effectively due to the absence of PDIA5, a rescue approach was undertaken. To this end an siRNA-resistant form of PDIA5 (PDIA5r) was expressed in HeLa cells silenced or not for PDIA5 and the expression of PDIA5 evaluated by immunoblotting (Fig. 3D). As expected, endogenous PDIA5 was silenced upon transfection with the siRNA to PDIA5 (Fig. 3D, lane 2) and the expression of the protein rescued when cotransfecting with the siRNA-resistant form (Fig. 3D, lane 3). To test whether rescuing PDIA5 expression impacted ATF6 α signaling, DTT-induced expression of *Ero1L β* and *Herpud1* mRNAs was monitored in cells knocked down for PDIA5 and rescued or not for the expression of this protein (Fig. 3E). Again, as shown in Fig. 3A and in Fig. S5 in the supplemental material, PDIA5 silencing led to attenuated induction of *Ero1L β* and *Herpud1* mRNA expression upon DTT exposure, and expression of PDIA5r in the silenced background restored the DTT-mediated induction of both mRNAs (Fig. 3E), thereby confirming PDIA5 dependency for ATF6 α signaling in HeLa cells. Interestingly, overexpression of PDIA5 alone was not sufficient to induce further expression of ATF6 α target genes, suggesting that endogenous PDIA5 is not limiting. Finally, the impact of PDIA5 silenc-

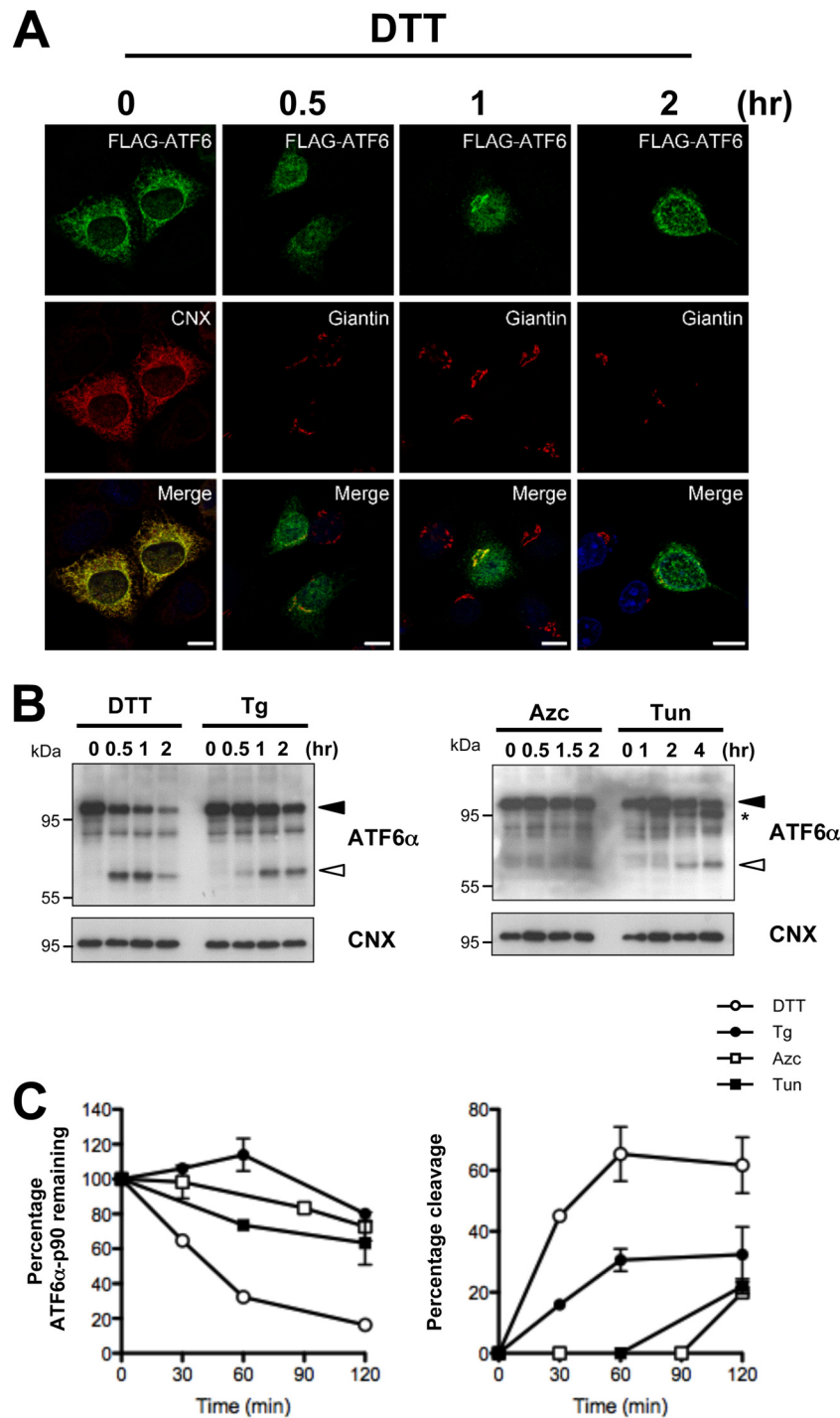


FIG 1 ATF6α activation assay. (A) HeLa cells were transfected with FLAG-ATF6α plasmid for 24 h and treated with 1 mM DTT for the indicated time. Cells were then immunostained with anti-FLAG and anti-CNX (for the ER) or antigiantin (for the Golgi apparatus) antibodies. Cells were analyzed by confocal microscopy. Bars, 10 μm. (B) Cleavage of endogenous ATF6α in HeLa cells exposed to DTT (1 mM), Tg (500 nM), Azc (10 mM), or Tun (5 μg/ml) as analyzed by immunoblotting using anti-ATF6α antibodies. The full-length (ATF6α-p90) and cleaved (ATF6α-p50) forms of ATF6α are indicated by black and white arrowheads, respectively. The asterisk shows the nonglycosylated form of ATF6α. Anti-CNX was used as loading control. (C) Time course quantification of ATF6α-p90 and ATF6α-p50 upon treatment with the indicated ER stressor.

ing on the expression of BiP protein, whose encoding gene is a major target of ATF6α, in response to ER stress was evaluated. When PDIA5 expression was knocked down in the cells, the induction of BiP upon ER stress was significantly attenuated compared to that with control siRNA (Fig. 4A; see Fig. S6 in the sup-

plemental material), thus indicating that PDIA5 might be indeed required for ATF6α activation and subsequent signaling.

PDIA5-dependent activation of ATF6α is independent of the association with BiP. As BiP has also been shown to control ATF6α export from the ER through a dissociation mechanism (6),

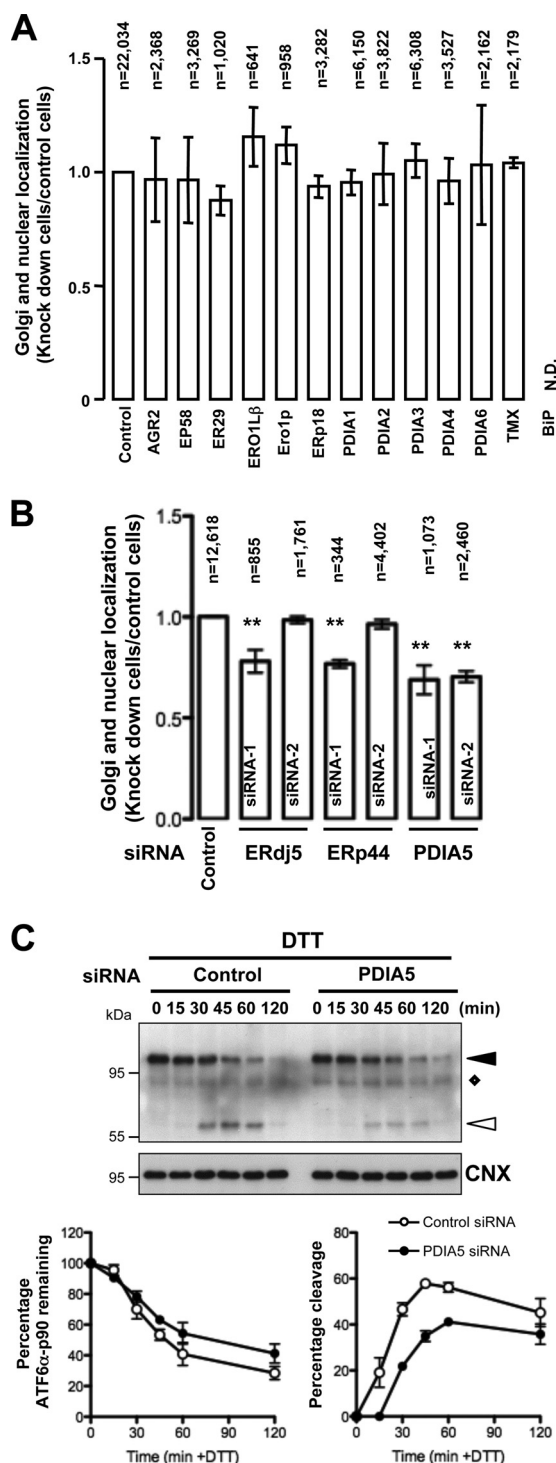


FIG 2 Small interfering RNA screen. (A) siRNA-based assay in HeLa cells. Following transfection with siRNAs (25 nM) and FLAG-ATF6 α plasmid, the cells were treated with DTT (1 mM) for 2 h and costained with antibodies against FLAG and CNX or giantin. The number of cells with Golgi apparatus and nuclear staining was counted using confocal or epifluorescence microscopy. The percentage of Golgi apparatus and nuclear localization in siRNA-transfected cells was calculated and compared with that in control siRNA-transfected cells. Data are the mean \pm SEM from triplicate experiments. *n*, number of cells counted for each siRNA experiment. N.D., not determined. (B) Secondary screen using alternative siRNA against targets identified in the primary screen. **, *P* < 0.01 (compared with control). (C) siRNAs against

we sought to examine if there was any functional interplay between BiP dissociation and the PDIA5 effect on ATF6 α . To this end, the ATF6 α /BiP interaction was tested by coimmunoprecipitation. To prevent the export of ATF6 α from the ER, and therefore its cleavage, the experiments were carried out in HeLa cells transfected with a dominant negative Sar1 [Sar1(DN)] construct, a mutant GTPase that prevents ER-to-Golgi traffic (20). Under those circumstances, BiP associated with ATF6 α under basal conditions and was released from ATF6 α upon DTT treatment (Fig. 4B). The same phenomenon was observed in PDIA5-silenced cells, although to a lesser extent (Fig. 4B and C). This suggests that dissociation of BiP from ATF6 α might represent an early step in the ATF6 α activation process but one not completely sufficient to allow ATF6 α export to the Golgi complex.

Modulation of disulfide bonds underlies PDIA5 activation of ATF6 α . Since our results showed that the export of ATF6 α from the ER was regulated by PDIA5 upon ER stress and since its activation is in part controlled by modulation of disulfide bonds (7), we then evaluated the oligomerization of ATF6 α using nonreducing (NR) SDS-PAGE and immunoblotting (Fig. 4D). This revealed that DTT treatment altered dramatically the ATF6 α oligomeric profile in control cells (Fig. 4D, left panel), whereas in PDIA5 siRNA-transfected cells, the high-molecular-weight forms remained present throughout the stress (Fig. 4D, right panel; see Fig. S7 in the supplemental material). To evaluate the impact of PDIA5 silencing on the formation of disulfide bonds in ATF6 α , FLAG-ATF6 α was immunoprecipitated and the reduced-cysteine-containing peptides C1 and C2 (Fig. 4E, left panel) were quantified by mass spectrometry (Fig. 4E, right panel). This revealed that both peptides C1 and C2 were found in equivalent amounts under all experimental conditions. However, the amount of C1 and C2 was dramatically decreased in PDIA5-silenced cells (Fig. 4E, right panel). This suggests that PDIA5 impacts the ATF6 α luminal domain content of reduced cysteines, thereby contributing to its activation process upon ER stress.

PDIA5 modulates ATF6 α packaging into COPII vesicles. The coat protein complex II (COPII) is required for packaging of ATF6 α and its trafficking from the ER to the Golgi complex upon ER stress (14). We therefore examined whether PDIA5 silencing impacted ATF6 α packaging into COPII vesicles. As previously reported (14), ATF6 α budded poorly in the standard control reaction (Fig. 5A, lane 7). When DTT (5 mM) was added into the budding reaction mixtures, ATF6 α packaging into COPII vesicles was enhanced (Fig. 5A, lane 8), a phenomenon that was greatly suppressed in PDIA5-silenced cells (Fig. 5A, lane 10). In control experiments, DTT did not affect ERGIC53 or Sec22b budding and did not cause significant ribophorin I release, as previously reported for the initial assay (14). Collectively, these results indicate that PDIA5 plays an instrumental role in ATF6 α packaging to COPII vesicles. To further reinforce the functional link between PDIA5 and ATF6 α , we first evaluated whether the silencing of these two genes impacted the cell's sensitivity to ER stress. Both

PDIA5 were transfected into HeLa cells. Seventy-two hours after transfection, cells were treated with DTT (1 mM) for the indicated periods of time. Cell lysates were analyzed by immunoblotting using anti-ATF6 α antibody. ATF6 α -p90 and ATF6 α -p50 are indicated by black and white arrowheads, respectively. The diamond shows a nonspecific protein recognized by anti-ATF6 α antibodies. Time course quantifications of ATF6 α -p90 (left) and ATF6 α -p50 (right) upon treatment are shown in the lower graphs.

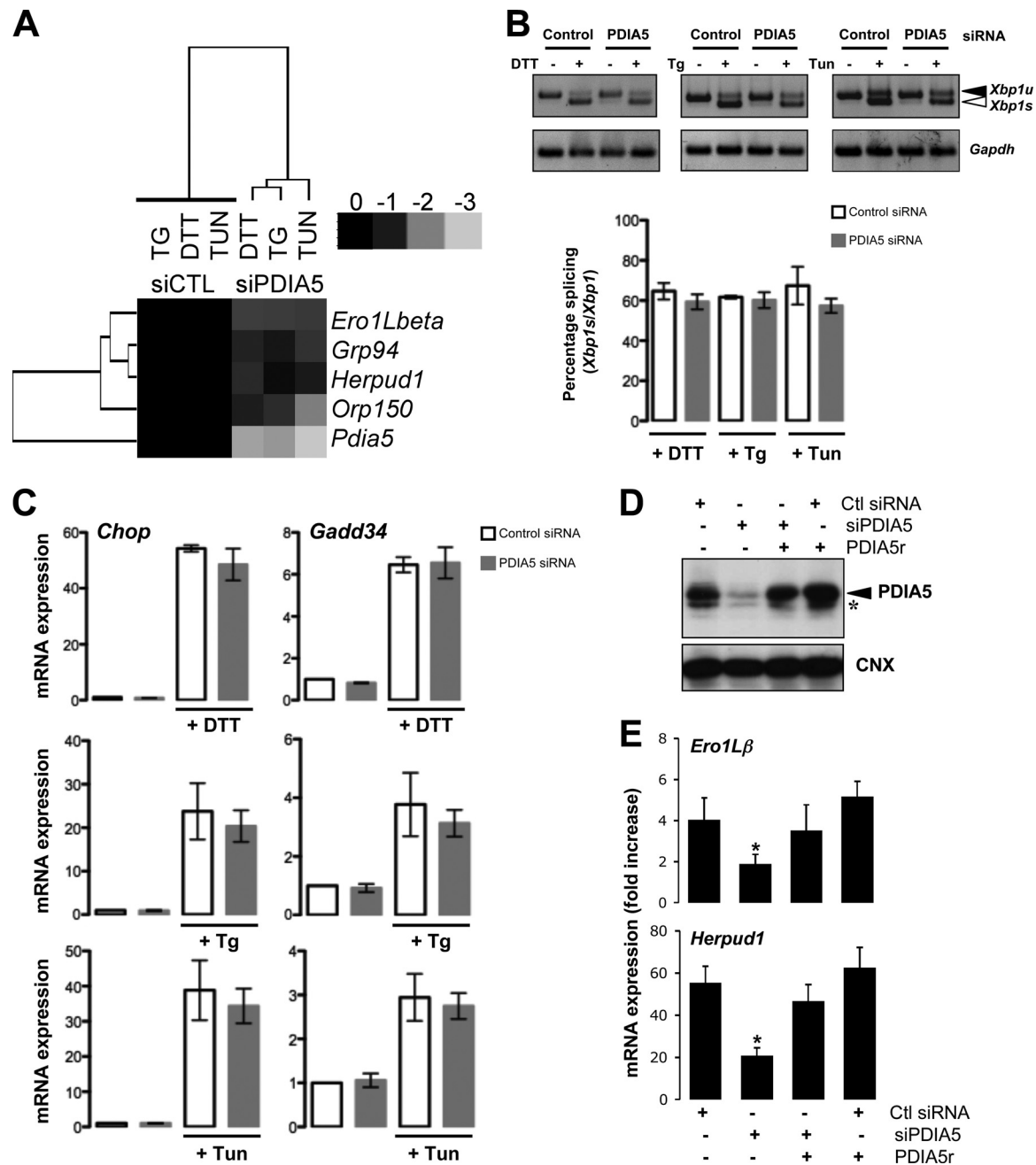


FIG 3 Effects of PDIA5 silencing on ATF6α target genes and UPR signaling. (A) Heat map representation of the expression of ATF6α target genes upon silencing of PDIA5 using siRNA (25 nM) in HeLa cells. Forty-eight hours after transfection, cells were treated with 1 mM DTT, 500 nM Tg, or 5 μg/ml Tun for 2 h. Total RNA was isolated and analyzed by qPCR using specific primers for ATF6α target genes (*Ero1Lβ*, *Grp94*, *Herpud1*, and *Orp150*). Expression of each mRNA was normalized to that of *Gapdh* mRNA. (B) HeLa cells were transfected with siRNA and treated with DTT, Tg, or Tun, and the splicing of *Xbp1* mRNA was evaluated using reverse transcription-PCR (RT-PCR). (C) RNA was extracted from control or PDIA5-silenced and ER-stressed HeLa cells and analyzed by qPCR using the specific primers *Gadd34*, *Chop*, and *Gapdh*. Data for qPCR are the mean ± standard deviation (SD) from three independent experiments. (D) HeLa cells were transfected with siRNA (control [Ctl] or PDIA5) and further transfected with pcDNA3-PDIA5r or not. Forty-eight hours later, lysates were analyzed by immunoblotting using either anti-PDIA5 or anti-CN X antibodies. The arrowhead shows PDIA5, and the asterisk indicates a nonspecific band. (E) Cells transfected as for panel D were then treated with 1 mM DTT for 2 h or not treated. RNA was then extracted, and the expression of *Ero1Lβ* and *Herpud1* was evaluated by qPCR. Data are the average from three independent experiments ± SEM. *, *P* < 0.05.

PDIA5 and ATF6α silencing increased Tun toxicity, with similar orders of magnitude (see Fig. S8 in the supplemental material). Moreover, we tested whether overexpression of the cytosolic part of ATF6α (ATF6α-p50), a constitutively activated form of ATF6α

independent of disulfide bond reduction, would rescue PDIA5 silencing-mediated ER stress sensitivity. HeLa cells were transfected with an empty vector or FLAG-ATF6α-p50 and treated with 5 μg/ml Tun or vehicle control for 36 h. The expression of

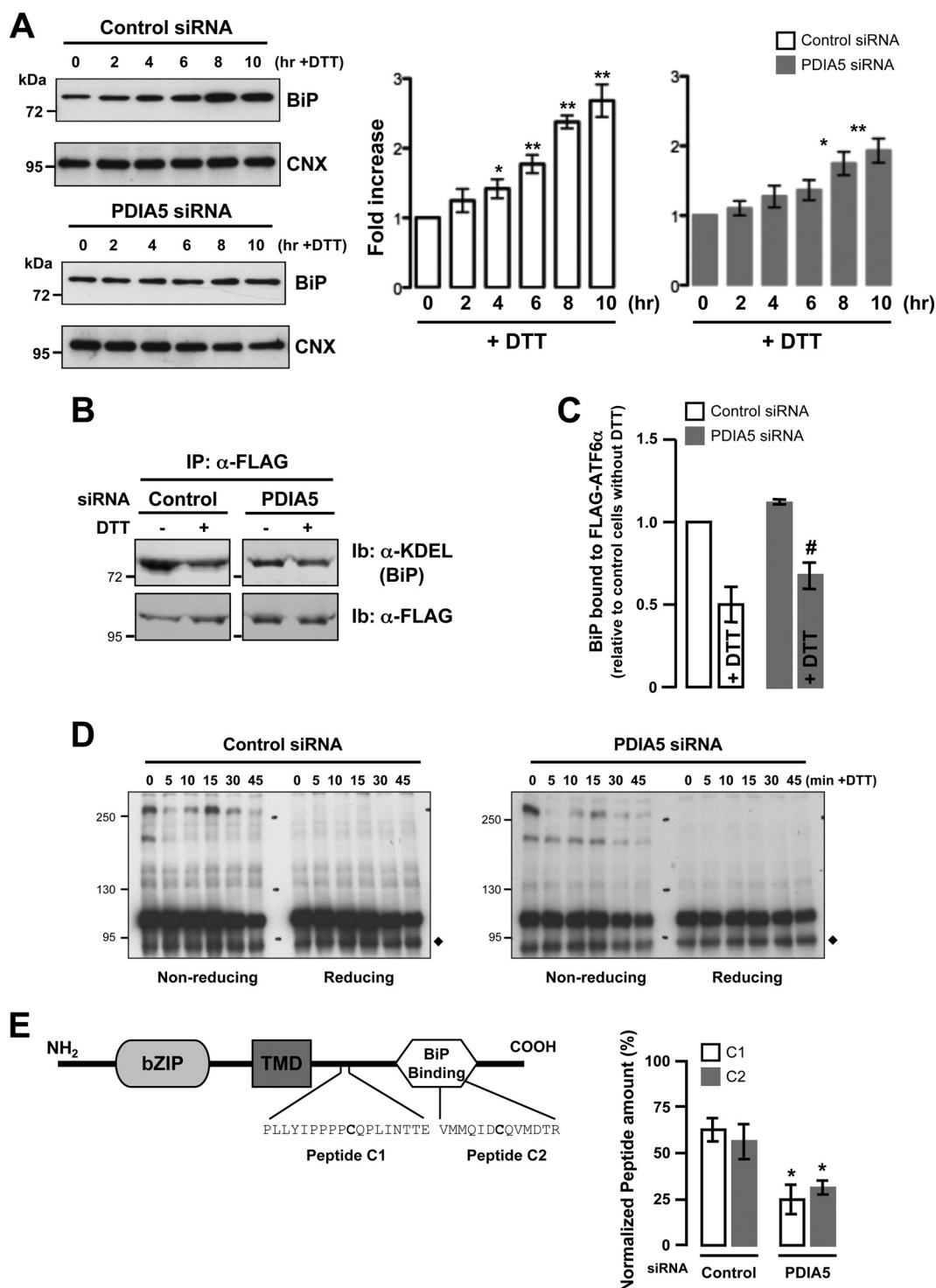


FIG 4 Effects of PDIA5 silencing on ATF6 α signaling. (A) At 72 h after PDIA5 siRNA transfection, HeLa cells were treated with 1 mM DTT for the indicated periods of time. BiP protein expression was analyzed by immunoblotting using anti-KDEL antibody (left panels). Anti-CN α antibodies were used as a loading control. BiP expression was normalized to CN α expression and quantified as a percentage of the signal at time zero (right panels). *, $P < 0.05$; **, $P < 0.01$ (compared to the signal at time zero). (B) HeLa-ATF6 α cells were transfected with PDIA5 siRNA for 72 h and with Sar1(DN) for 24 h. Cell lysates were prepared from the cells treated with or without DTT (1 mM for 1 h) and immunoprecipitated (IP) using anti-FLAG antibody. Immunoprecipitates were resolved by SDS-PAGE and immunoblotted (Ib) using anti-KDEL and anti-FLAG antibodies. (C) Quantification of BiP and FLAG-ATF6 α . Means \pm SEM from triplicate experiments are shown. #, $P < 0.03$ compared with control. (D) Analysis of ATF6 α redox state under conditions of PDIA5 silencing and ER stress. The diamond shows a nonspecific protein. (E) Left panel, schematic representation of ATF6 α , including the cytosolic domain containing the DNA binding site, the transmembrane domain, and the luminal domain with the BiP binding site. In the luminal domain, the two cysteine-containing peptides as generated by trypsin and GluC proteolytic cleavage are indicated (peptides C1 and C2). Right panel, quantification of peptides C1 and C2 in HeLa-ATF6 α cells transfected with siRNA against PDIA5 under basal conditions. Normalization was performed using three other ATF6 α cysteine-free peptides identified and quantified under the same experimental conditions.

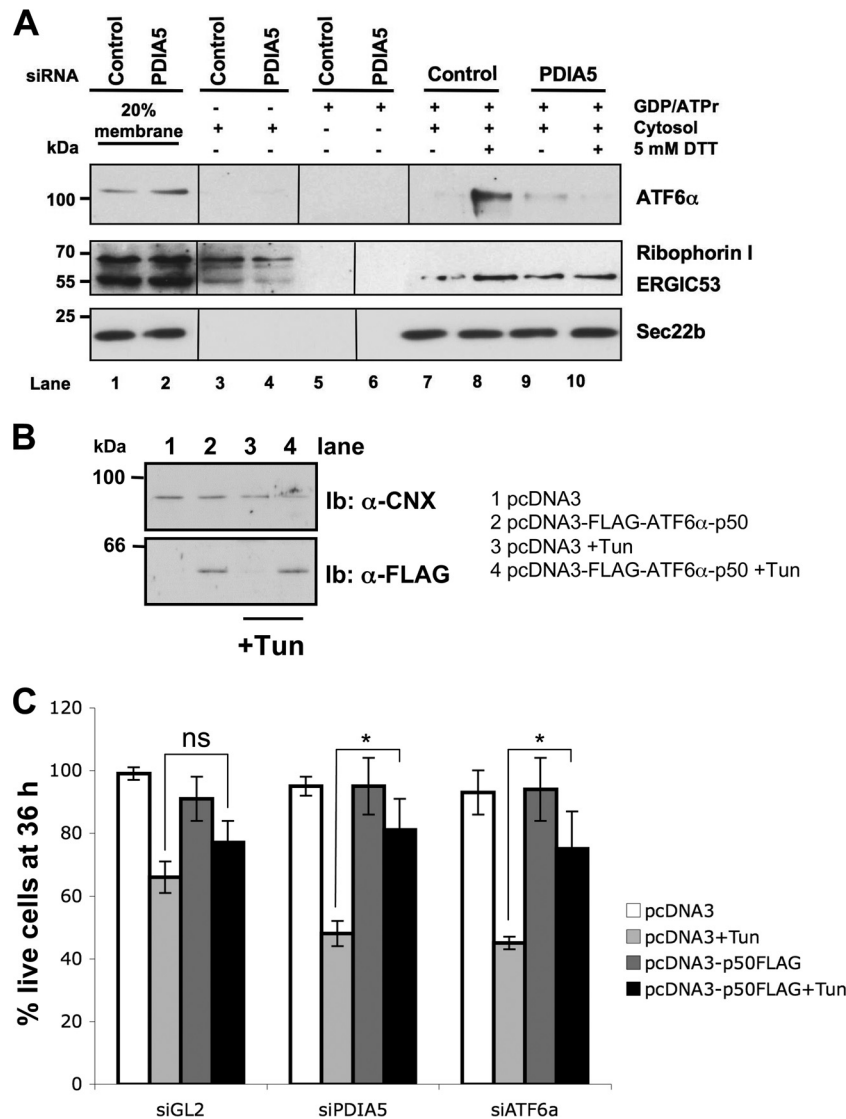


FIG 5 ATF6α export and PDIA5-mediated sensitivity to ER stress. (A) ATF6α export reconstitution assay. Vesicular fractions obtained from control siRNA-treated HeLa-ATF6α cells and from cells silenced for PDIA5 for 72 h were analyzed by immunoblotting using anti-ATF6α, anti-ribophorin I, anti-ERGIC53, and anti-Sec22b antibodies. (B) HeLa cells were transfected with empty pcDNA3 vector or pcDNA3-FLAG-ATF6α-p50. Twenty-four hours posttransfection, cells were treated with Tun (5 μg/ml) for 36 h. Cell lysates were extracted and analyzed by immunoblotting using anti-FLAG antibody. CNX was used as a loading control. (C) Empty pcDNA3 or pcDNA3-FLAG-ATF6α-p50 was transiently transfected in HeLa cells as for panel B. Twenty-four hours posttransfection, cells were treated with 5 μg/ml Tun for 36 h, and a cell toxicity assay based on SRB staining was performed. Data are shown as the means from three independent experiments ± SEM. *, $P < 0.05$; ns, no significant difference.

FLAG-ATF6α-p50 was monitored using immunoblotting with anti-FLAG antibodies (Fig. 5B, bottom panel). The same experiment was repeated in PDIA5- or ATF6α-silenced cells. The results presented in Fig. 5C show ATF6α-p50 rescued partially stress Tun sensitivity induced upon PDIA5 or ATF6α silencing. These results further support the functional link existing between these two proteins in the UPR.

The PDIA5/ATF6α axis modulates sensitivity to imatinib. ATF6α and PDIA5 have been associated with cell survival and chemoresistance in different tumor types (21, 22). Using leukemia as a model, we sought to determine the role of this newly identified axis in chemoresistance, a well-defined ER stress inducer. We initially examined the expression of *Pdia5* mRNA in leukemia cell lines K562 and LAMA (sensitive or resistant to imatinib). Expres-

sion of *Pdia5* mRNA was significantly higher in resistant cells than in sensitive cells (Fig. 6A), and it was not induced upon imatinib treatment (Fig. 6B). To evaluate the impact of PDIA5 expression on the resistance phenotype, PDIA5 expression was silenced or not in K562R cells, which were then subjected to imatinib treatment. Interestingly, PDIA5 silencing in K562R cells partially restored the cells' sensitivity to imatinib to a level comparable to that observed in sensitive cells (Fig. 6C). Furthermore, this effect was mimicked when using a pharmacological inhibitor of PDI (16F16) (Fig. 6D). To test whether overexpression of PDIA5 was functionally linked to ATF6α activation in K562R cells, ATF6α expression was knocked down using siRNA and the subsequent impact on imatinib sensitivity evaluated. Interestingly, ATF6α silencing partially restored the sensitivity of K562R cells to imatinib (Fig. 7A),

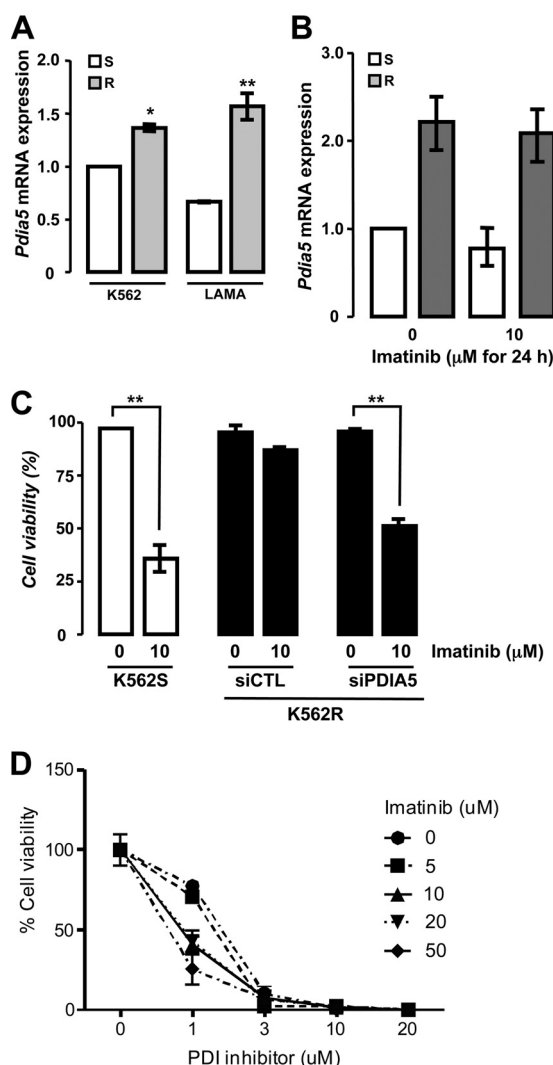


FIG 6 Expression and function of PDIA5 in imatinib-sensitive and -resistant leukemia cells. (A) Expression of *Pdia5* mRNA in K562 and LAMA cells either sensitive (S) or resistant (R) to imatinib as determined by qPCR. Data are presented as the average from three independent experiments \pm SEM. *, $P < 0.05$; **, $P < 0.01$. (B) *Pdia5* mRNA expression in imatinib-sensitive or -resistant K562 cells subjected to imatinib (10 μ M) treatment. Data are presented as the average from three independent experiments \pm SD. (C) Cell viability in response to 10 μ M imatinib treatment was determined in imatinib-sensitive K562 cells (K562S) or in imatinib-resistant K562 cells (K562R) transfected with a control siRNA (siCTL) or with an siRNA against PDIA5 (siPDIA5). Data are presented as the average from three independent experiments \pm SEM. **, $P < 0.01$. (D) Impact of PDIA5 pharmacological inhibition with increasing concentrations of 16F16 on K562R cells' sensitivity to imatinib. Data are presented as the average from three independent experiments \pm SEM.

and a pharmacological inhibitor of PDI blocked the proteolytic cleavage of ATF6 α in those cells, which was found to be constitutive otherwise (Fig. 7B). Finally, the cosilencing of PDIA5 and ATF6 α further enhanced the sensitivity of K562R cells to imatinib (Fig. 7C), thereby demonstrating the functional relationship of these proteins in the chemoresistance mechanism. This observation was also confirmed in CD34⁺ leukemia cells from two patients (Fig. 7D), in which imatinib sensitivity was enhanced using

16F16, thereby reinforcing the pathophysiological and translational relevance of the PDIA5/ATF6 α axis in cancer.

DISCUSSION

The biological role of the UPR in oncogenesis, cancer development, and resistance to chemotherapies is well established; however, the roles of the three UPR sensors remain unequally documented. In particular, the role of ATF6 α is yet to be characterized. To define the mechanisms of activation of ATF6 α in cancer, we designed an siRNA screen aiming at identifying the proteins controlling ATF6 α export from the ER. The subsequent results defined a novel ER stress-inducible regulatory axis that depends on PDIA5-mediated activation of ATF6 α . In this context, and to follow up on our initial aim, we investigated the relevance of this axis to cancer cell phenotypes. Interestingly, PDIA5 was found to be overexpressed in numerous cancers and to be part of a predictive signature of tumor cell resistance to chemotherapy (21, 22); however, the mechanisms underlying this observation remain poorly understood. Since ATF6 α had previously been associated with tumor cell dormancy (11), a hallmark of chemotherapy resistance, we investigated the role of the PDIA5/ATF6 α axis in cancer cell resistance to imatinib. We showed that genetically or pharmacologically impairing PDIA5 activity restored imatinib sensitivity in imatinib-resistant leukemia K562 cells (Fig. 6 and 7) and that this was through an ATF6 α -dependent mechanism (Fig. 7 and 8). Thus, our data demonstrated the role of the PDIA5/ATF6 α signaling axis in the resistance of leukemia cells to imatinib. One can anticipate that such results might also be observable in other models of drug resistance in cancer cells.

We further elaborated on the molecular mechanisms underlying this phenomenon. It is currently accepted that the export of ATF6 α to the Golgi apparatus upon ER stress is controlled by the dissociation from the ER chaperone BiP (6) and that the remodelling of intra- and intermolecular disulfide bonds formed in the luminal domain of ATF6 α is also involved in its activation process (7, 8). We found that PDIA5 silencing caused the retention of ATF6 α in the ER under stress, thereby indicating that PDIA5 is involved in the ATF6 α activation mechanism upon ER stress. Silencing of PDIA5 did not significantly affect the activation of the other arms of the UPR. These results suggest possible mechanisms of PDIA5-dependent reduction of ATF6 α , including (i) direct reduction that could be further evaluated by the detection of a mixed-disulfide ATF6 α -PDIA5 species or, alternatively, by *in vitro* catalysis of ATF6 α reduction using a reconstituted system and (ii) indirect reduction via hypo-oxidizing ER conditions, which could be assessed by measuring the thiol-disulfide milieu in the ER in control or PDIA5-silenced cells.

It has been clearly demonstrated in previous reports that select protein complexes were essential to the fine regulation of IRE1 signaling (23). This protein platform, named the UPRosome, is essential for controlling IRE1-dependent cell fate decisions upon ER stress (24, 25). In view of the results presented here, one can propose the emergence of the UPRosome as a general concept to regulate the ER stress sensors and consequently the cellular outcome resulting from their activation. In the case of ATF6 α , the complex(es) formed with PDIA5 (this study) and BiP (6) in the ER might represent the first example of an expanding family of UPRosome platforms controlling UPR function.

In the present study, we also showed that ATF6 α dissociation from BiP, the first event occurring in response to ER stress, is

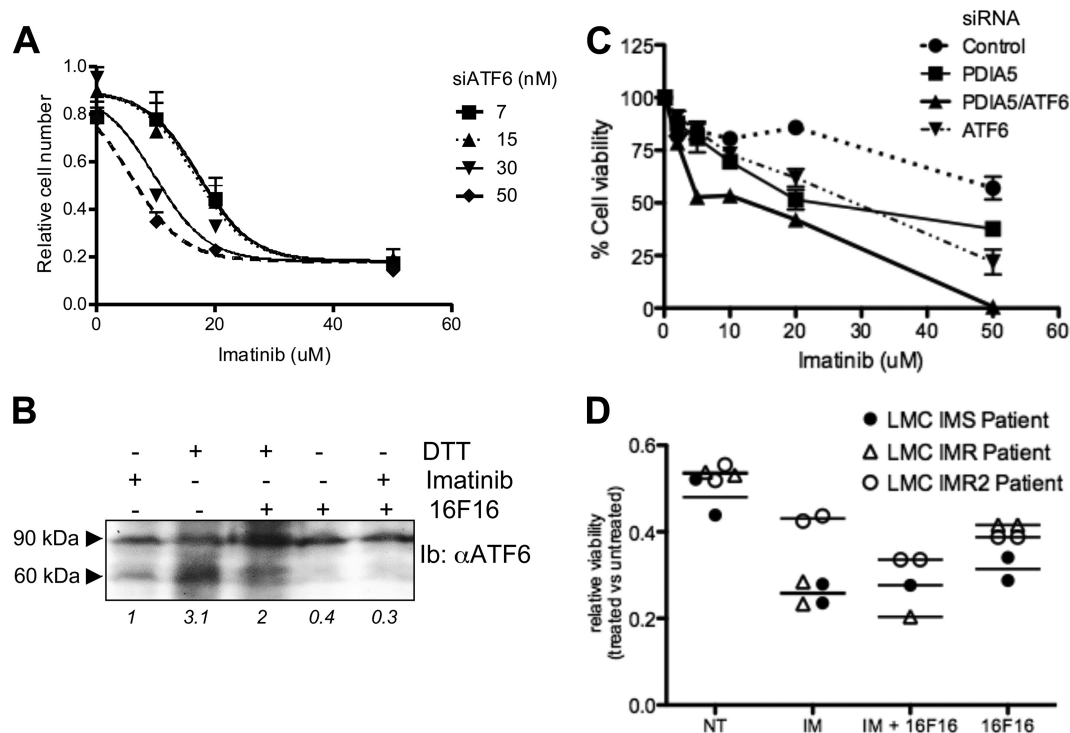


FIG 7 Genetic and pharmacological disruption of the PDIA5/ATF6 α signaling axis in K562 and patient-derived leukemia cells. (A) Impact of ATF6 α siRNA-mediated silencing on K562R cells' sensitivity to imatinib. Seventy-two hours after transfection, cells were treated with the indicated concentration of imatinib for 48 h. Data are presented as the average from three independent experiments \pm SEM. (B) Impact of PDIA5 pharmacological inhibition with 16F16 on ATF6 α proteolytic processing in K562R cells subjected to imatinib and/or DTT treatment as assessed by immunoblotting using anti-ATF6 α antibodies. (C) Impact of ATF6 α and/or PDIA5 siRNA-mediated silencing on K562R cells' sensitivity to imatinib. Data are presented as the average from three independent experiments \pm SEM. (D) Impact of PDIA5 pharmacological inhibition with 16F16 on imatinib sensitivity in three patient-derived leukemia lines either sensitive (IMS, CD34 $^{-}$) or resistant (IMR, CD34 $^{+}$) to imatinib.

necessary but not sufficient for ATF6 α export. Interestingly, the BiP binding site on ATF6 α on amino acids 467 to 475 (6) also encompasses a cysteine residue (peptide C2 [Fig. 5D]) that is important for the ATF6 α activation process (reference 6 and this

study). The dissociation from BiP could therefore represent an early/upstream event in the process that could occur in conjunction with cysteine oxidation to favor its activation. Finally, the expression of exogenous ATF6 α -p50 is sufficient to rescue the

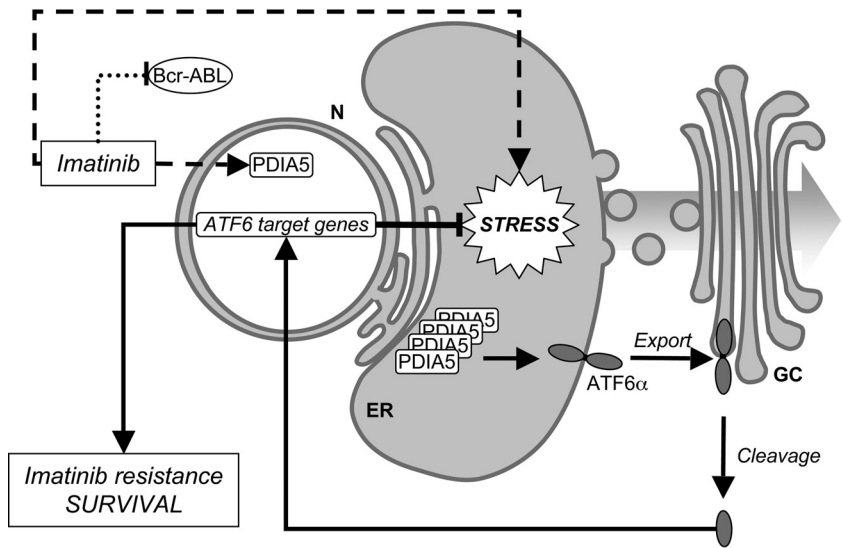


FIG 8 Schematic representation of the role of the PDIA5/ATF6 α signaling axis in chemoresistance in leukemia cells. Arrows represent activation pathways, whereas inhibitory mechanisms are represented by T-bars. Broken lines represent pathways with uncharacterized mechanisms.

activation deficiency observed upon PDIA5 silencing and the resulting increased sensitivity of cells to ER stress (Fig. 5).

In conclusion, our results shed light on novel mechanisms that are responsible for the control of ATF6 α activation through redox mechanisms and contribute to specific ER stress-induced signaling loops (26), and they link this mechanism to the yet incompletely understood mechanisms of resistance to chemotherapy. Moreover, this study, by expanding the repertoire of molecular intermediates involved in the regulation of ER stress signaling, provides additional drug targets to bypass resistance to chemotherapy in cancer cells.

ACKNOWLEDGMENTS

We thank K. Dejgaard (McGill University, Montreal, Quebec, Canada) and the Bordeaux Proteomics Platform for mass spectrometry sequencing.

This work was supported by grants from INSERM (Avenir), Ligue contre le Cancer (Comité des Landes), and Institut National du Cancer (INCa) to E.C., a Ulysses/IRCSET grant to E.C. and J.C.S., and funds from the Howard Hughes Medical Institute to R.S. S.L. was supported by a Ph.D. scholarship from the French government.

We declare no conflict of interest.

REFERENCES

- Ron D, Walter P. 2007. Signal integration in the endoplasmic reticulum unfolded protein response. *Nat. Rev. Mol. Cell. Biol.* 8:519–529. <http://dx.doi.org/10.1038/nrm2199>.
- Harding HP, Zhang Y, Ron D. 1999. Protein translation and folding are coupled by an endoplasmic-reticulum-resident kinase. *Nature* 397:271–274. <http://dx.doi.org/10.1038/16729>.
- Yoshida H, Matsui T, Yamamoto A, Okada T, Mori K. 2001. XBP1 mRNA is induced by ATF6 and spliced by IRE1 in response to ER stress to produce a highly active transcription factor. *Cell* 107:881–891. [http://dx.doi.org/10.1016/S0092-8674\(01\)00611-0](http://dx.doi.org/10.1016/S0092-8674(01)00611-0).
- Hollien J, Lin JH, Li H, Stevens N, Walter P, Weissman JS. 2009. Regulated Ire1-dependent decay of messenger RNAs in mammalian cells. *J. Cell Biol.* 186:323–331. <http://dx.doi.org/10.1083/jcb.200903014>.
- Haze K, Yoshida H, Yanagi H, Yura T, Mori K. 1999. Mammalian transcription factor ATF6 is synthesized as a transmembrane protein and activated by proteolysis in response to endoplasmic reticulum stress. *Mol. Biol. Cell* 10:3787–3799. <http://dx.doi.org/10.1091/mbc.10.11.3787>.
- Shen J, Chen X, Hendershot L, Prywes R. 2002. ER stress regulation of ATF6 localization by dissociation of BiP/GRP78 binding and unmasking of Golgi localization signals. *Dev. Cell* 3:99–111. [http://dx.doi.org/10.1016/S1534-5807\(02\)00203-4](http://dx.doi.org/10.1016/S1534-5807(02)00203-4).
- Nadanaka S, Okada T, Yoshida H, Mori K. 2007. Role of disulfide bridges formed in the luminal domain of ATF6 in sensing endoplasmic reticulum stress. *Mol. Cell. Biol.* 27:1027–1043. <http://dx.doi.org/10.1128/MCB.00408-06>.
- Nadanaka S, Yoshida H, Mori K. 2006. Reduction of disulfide bridges in the luminal domain of ATF6 in response to glucose starvation. *Cell Struct. Funct* 31:127–134. <http://dx.doi.org/10.1247/csf.06024>.
- Arai M, Kondoh N, Imazeki N, Hada A, Hatsuse K, Kimura F, Matsubara O, Mori K, Wakatsuki T, Yamamoto M. 2006. Transformation-associated gene regulation by ATF6 α during hepatocarcinogenesis. *FEBS Lett.* 580:184–190. <http://dx.doi.org/10.1016/j.febslet.2005.11.072>.
- Malhi H, Kaufman RJ. 2011. Endoplasmic reticulum stress in liver disease. *J. Hepatol.* 54:795–809. <http://dx.doi.org/10.1016/j.jhep.2010.11.005>.
- Schewe DM, Aguirre-Ghiso JA. 2008. ATF6 α -Rheb-mTOR signaling promotes survival of dormant tumor cells in vivo. *Proc. Natl. Acad. Sci. U. S. A.* 105:10519–10524. <http://dx.doi.org/10.1073/pnas.0800939105>.
- Chevet E, Cameron PH, Pelletier MF, Thomas DY, Bergeron JJ. 2001. The endoplasmic reticulum: integration of protein folding, quality control, signaling and degradation. *Curr. Opin. Struct. Biol.* 11:120–124. [http://dx.doi.org/10.1016/S0959-440X\(00\)00168-8](http://dx.doi.org/10.1016/S0959-440X(00)00168-8).
- Moenner M, Pluquet O, Bouchecareilh M, Chevet E. 2007. Integrated endoplasmic reticulum stress responses in cancer. *Cancer Res.* 67:10631–10634. <http://dx.doi.org/10.1158/0008-5472.CAN-07-1705>.
- Schindler AJ, Schekman R. 2009. In vitro reconstitution of ER-stress induced ATF6 transport in COPII vesicles. *Proc. Natl. Acad. Sci. U. S. A.* 106:17775–17780. <http://dx.doi.org/10.1073/pnas.0910342106>.
- Kim J, Hamamoto S, Ravazzola M, Orci L, Schekman R. 2005. Uncoupled packaging of amyloid precursor protein and presenilin 1 into coat protein complex II vesicles. *J. Biol. Chem.* 280:7758–7768. <http://dx.doi.org/10.1074/jbc.M411091200>.
- Mouton-Barbosa E, Roux-Dalvai F, Bouyssie D, Berger F, Schmidt E, Righetti PG, Guerrier L, Boschetti E, Burlet-Schiltz O, Monsarrat B, Gonzalez de Peredo A. 2010. In-depth exploration of cerebrospinal fluid by combining peptide ligand library treatment and label-free protein quantification. *Mol. Cell Proteomics* 9:1006–1021. <http://dx.doi.org/10.1074/mcp.M900513-MCP200>.
- Dejeans N, Pluquet O, Lhomond S, Grise F, Bouchecareilh M, Juin A, Meynard-Cadars M, Bidaud-Meynard A, Gentil C, Moreau V, Saltel F, Chevet E. 2012. Autocrine control of glioma cells adhesion and migration through IRE1 α -mediated cleavage of SPARC mRNA. *J. Cell Sci.* 125:4278–4287. <http://dx.doi.org/10.1242/jcs.099291>.
- Adachi Y, Yamamoto K, Okada T, Yoshida H, Harada A, Mori K. 2008. ATF6 is a transcription factor specializing in the regulation of quality control proteins in the endoplasmic reticulum. *Cell Struct. Funct* 33:75–89. <http://dx.doi.org/10.1247/csf.07044>.
- Yamamoto K, Sato T, Matsui T, Sato M, Okada T, Yoshida H, Harada A, Mori K. 2007. Transcriptional induction of mammalian ER quality control proteins is mediated by single or combined action of ATF6 α and XBP1. *Dev. Cell* 13:365–376. <http://dx.doi.org/10.1016/j.devcel.2007.07.018>.
- Nakano A, Otsuka H, Yamagishi M, Yamamoto E, Kimura K, Nishikawa S, Oka T. 1994. Mutational analysis of the Sar1 protein, a small GTPase which is essential for vesicular transport from the endoplasmic reticulum. *J. Biochem.* 116:243–247.
- Beesley AH, Firth MJ, Anderson D, Samuels AL, Ford J, Kees UR. 2013. Drug-gene modeling in pediatric T-cell acute lymphoblastic leukemia highlights importance of 6-mercaptopurine for outcome. *Cancer Res.* 73:2749–2759. <http://dx.doi.org/10.1158/0008-5472.CAN-12-3852>.
- Burguillo FJ, Martin J, Barrera I, Bardsley WG. 2010. Meta-analysis of microarray data: the case of imatinib resistance in chronic myelogenous leukemia. *Comput. Biol. Chem.* 34:184–192. <http://dx.doi.org/10.1016/j.compbiolchem.2010.06.003>.
- Hetz C, Glimcher LH. 2009. Fine-tuning of the unfolded protein response: assembling the IRE1 α interactome. *Mol. Cell* 35:551–561. <http://dx.doi.org/10.1016/j.molcel.2009.08.021>.
- Hetz C. 2012. The unfolded protein response: controlling cell fate decisions under ER stress and beyond. *Nat. Rev. Mol. Cell. Biol.* 13:89–102.
- Hetz C, Martinon F, Rodriguez D, Glimcher LH. 2011. The unfolded protein response: integrating stress signals through the stress sensor IRE1 α . *Physiol. Rev.* 91:1219–1243. <http://dx.doi.org/10.1152/physrev.00001.2011>.
- Higa A, Chevet E. 2012. Redox signaling loops in the unfolded protein response. *Cell Signal.* 24:1548–1555. <http://dx.doi.org/10.1016/j.cellsig.2012.03.011>.